Numerical characterization of Love waves dispersion in viscoelastic guiding-layer under viscous fluid

Jérémy Bonhomme, Mourad Oudich, Pedro Alberto Segura Chavez, Mohamed Lamine Fayçal Bellaredj, Jean-François Bryche, D. Beyssen, Paul G Charette, Frédéric Sarry

RESEARCH ARTICLE | OCTOBER 20 2020

Numerical characterization of Love waves dispersion in viscoelastic guiding-layer under viscous fluid

Jérémy Bonhomme ; Mourad Oudich ; Pedro Alberto Segura Chavez ;
Mohamed Lamine Fayçal Bellaredj; Jean-François Bryche ; Denis Beyssen; Paul G. Charette; Frédéric Sarry

J. Appl. Phys. 128, 154502 (2020)
https://doi.org/10.1063/5.0022797

Journal of Applied Physics ARTICLE scitation.org/journal/jap

Numerical characterization of Love waves dispersion in viscoelastic guiding-layer under viscous fluid

Cite as: J. Appl. Phys. **128**, 154502 (2020); doi: 10.1063/5.0022797
Submitted: 23 July 2020 · Accepted: 23 September 2020 ·
Published Online: 20 October 2020

Jérémy Bonhomme,[1,2,3,4,a)] Mourad Oudich,[1,2,5,a)] Pedro Alberto Segura Chavez,[1,2,3,4] Mohamed Lamine Fayçal Bellaredj,[1,2] Jean-François Bryche,[3,4] Denis Beyssen,[1,2] Paul G. Charette,[3,4] and Frédéric Sarry[1,2]

AFFILIATIONS

[1]CNRS, Institut Jean Lamour, UMR 7198, Nancy F-54000, France
[2] Institut Jean Lamour, Université de Lorraine, UMR 7198, Nancy 54000, France
[3]Laboratoire Nanotechnologies Nanosystèmes (LN2)—CNRS UMI-3463, Université de Sherbrooke, Sherbrooke, Québec J1K 2R1, Canada
[4]Institut Interdisciplinaire d'Innovation Technologique (3IT), Université de Sherbrooke, Sherbrooke, Québec J1K 2R1, Canada
[5]Graduate Program in Acoustics, Penn State University, State College, Pennsylvania 16801, USA

[a)]**Authors to whom correspondence should be addressed:** jeremy.bonhomme@univ-lorraine.fr and mourad.oudich@univ-lorraine.fr

ABSTRACT

We present a finite element (FE) based model to accurately investigate the dispersion and attenuation of Love waves in a multilayered structure made of a piezoelectric substrate, a guiding layer, and a viscous fluid. The numerical model solves the general form of the wave equations that includes the materials anisotropy, piezoelectricity, and viscoelasticity. We express the wave equations for elastic waves in a particular formulation in order to solve an eigenvalue problem where the eigenvalue is the complex wavenumber k from which we can derive the phase velocity $[\omega/\mathrm{Re}(k)]$ and the attenuation rate $[\mathrm{Im}(k)]$. The numerical model enables us to study the effects of the interdigitated electrodes, the materials viscoelasticity and piezoelectricity, and the fluid's viscosity on the wave phase velocity and attenuation. Our FE based model will facilitate optimizing the design of anisotropic piezoelectric platforms for Love waves propagation under viscous fluid loading.

I. INTRODUCTION

Surface acoustic waves (SAWs) are commonly used for sensing in countless application areas, thanks to their wide operating frequency range and high sensitivity.[1–3] Particularly, in the field of bio-sensing, horizontally polarized and surface polarized shear SAWs were first introduced as efficient mechanisms to detect biomolecules in aqueous solutions with high sensitivity. Later on, Love waves (L-SAWs) based devices were developed using a guiding layer (GL) on the surface of piezoelectric substrates. This kind of wave is mostly confined within the guiding layer with shear horizontal motion, which significantly reduces its attenuation from energy leakage into the bio-fluid in contact with the guiding layer. This development was accompanied by rapid progress in sensing films and microfluidic technologies, all inserted in compact systems known as lab-on-a-chip.[4–7] At the same time, the need of optimizing the sensing performance of SAW has spurred the development of models and analytical methods to model the propagation of Love waves in multi-layered structures.[8–10] Later on, these models were extended to include the effects of fluid loading and viscosity on the phase velocity and wave attenuation.[11–14] However, the proposed analytical formulations were limited to perfectly layered geometrical structures and the wave equation was only solved for the zero-order Love waves.[11,15,16] Besides, simplifications were made upon the materials which were considered isotropic and

piezoelectricity was neglected. Furthermore, the interdigitated electrodes (IDTs) mass and shape effects were omitted, assuming a small electrode thickness compared to the operating wavelength. In addition, it is difficult to theoretically characterize the dispersion of Love waves and their attenuation in viscous media for the case of thin film surfaces with roughness or periodic structures; thus, numerical methods are to be constructed to deal with this kind of problem. In this paper, we introduce a finite element (FE) based model to study accurately the dispersion of Love waves under viscous liquid. The model includes the materials anisotropy, piezoelectricity, and viscoelasticity, along with the strong feature of solving the wave equations for a layered system that includes IDTs.

In the classical wave equations with constant parameters, eigen-frequency analysis is conducted to retrieve the relationship between the wave number k and the angular frequency ω in order to characterize the wave dispersion. However, including the materials viscoelasticity and fluid viscosity means considering frequency-dependent parameters, which constrains the construction of the eigenfrequency problem. To overcome this limitation, we consider solving the wave equation in the "wavenumber domain" instead of the angular frequency domain.[17] The frequency is considered an input parameter and the equations are changed to solve a new eigenvalue problem where the wavenumber k is the eigenvalue. We use this formulation in a FE based model to evaluate the complex wavenumber which is directly related to the phase velocity and attenuation of the wave for each operating frequency. The model offers the possibility to have more flexibility in terms of geometrical shape while allowing to easily change the materials' properties (anisotropy, piezoelectricity, and viscoelasticity) and the fluid viscosity. Furthermore, the mass effect of the electrodes used to excite the Love wave can be included in the model, which is a real advantage compared to the existing models.

We first present in Sec. II the governing equations of wave propagation in a multilayered structure made of a piezoelectric substrate, an isotropic guiding layer (GL), and a viscous fluid. We rewrite these equations in an adequate formulation that allows us to isolate the wave number as an eigenvalue for a specific frequency. Section III presents the evaluation results of the L-SAW phase velocity and attenuation for a silica GL on a quartz substrate, while a comparison is made with the results derived from the analytic model of Kiełczyński.[14] The final section presents applications for realistic cases that involve the anisotropy and piezoelectric propriety of the substrate such as $LiNbO_3$, the viscoelasticity of a polymeric GL, and an investigation about the effect of the electrodes on the Love wave phase velocity and attenuation.

II. THE WAVENUMBER-EIGENVALUE PROBLEM

We first consider the well-known platform for the propagation of a Love wave, composed of a semi-infinite piezoelectric substrate, a thin elastic GL with thickness denoted w, and a viscous fluid layer [Fig. 1(a)]. The objective is to numerically characterize the Love wave dispersion and investigate its attenuation caused by the viscous fluid. The mechanical and electrical behaviors of our system is described by the displacement field $\boldsymbol{u}$ and the electric

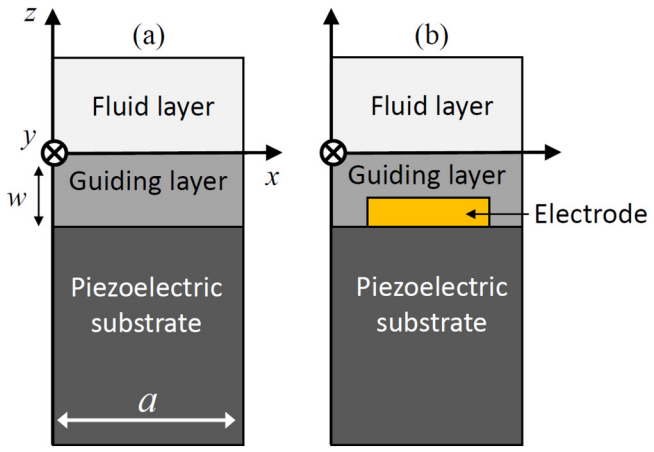

FIG. 1. Two-dimensional schematic representation of the multilayer structure made of a piezoelectric semi-infinite substrate, a guiding layer with thickness w, and a fluid layer. In our model, we have considered a system without an electrode (a) and with an electrode (b).

potential φ for a piezoelectric material,

$$\boldsymbol{u} = \begin{pmatrix} u_x(x,z,t) \\ u_y(x,z,t) \\ u_z(x,z,t) \end{pmatrix}, \quad \varphi(x,z,t), \tag{1}$$

where u_x, u_y, u_z are the displacement field components in the x, y, and z directions, respectively. As the propagation is along the x direction while the system is considered to be infinite in the y direction, these variables only depend on the space coordinates x and z. The elastodynamic and electrical induction equations for the piezoelectric substrate can be written as[18]

$$\rho \frac{\partial^2 u_i}{\partial t^2} = \frac{\partial T_{ij}}{\partial x_j}, \quad \frac{\partial D_j}{\partial x_j} = 0, \tag{2}$$

where

$$\begin{aligned} T_{ij} &= C_{ijkl}\frac{\partial u_l}{\partial x_k} + e_{kij}\frac{\partial \varphi}{\partial x_k}, \\ D_j &= e_{jkl}\frac{\partial u_l}{\partial x_k} - \varepsilon_{jk}\frac{\partial \varphi}{\partial x_k}, \end{aligned} \tag{3}$$

with $(i, j, k, l) \in \{1; 2; 3\}$ are indexes for the three directions in space, $x_1 = x$, $x_2 = y$, $x_3 = z$, T_{ij} are the components of the stress tensor, D_j are the components of the electrical displacement field, e_{kil} are the piezoelectric coefficients, ε_{jk} are the dielectric permittivity coefficients, c_{ijkl} are the elastic constants, and ρ is the mass density.

As we consider the system in two dimensions, the derivatives with respect to the y-axis vanish. Moreover, we only focus on Love waves and we solve the equations for the displacement along the

$x_2 = y$ direction. Equations (2) and (3) can be developed to

$$\begin{aligned}\rho\frac{\partial^2 u_y}{\partial t^2} &= \frac{\partial T_{21}}{\partial x} + \frac{\partial T_{23}}{\partial z},\ e_{16}\frac{\partial^2 u_y}{\partial x^2} + e_{14}\frac{\partial^2 u_y}{\partial x \partial z} + e_{36}\frac{\partial^2 u_y}{\partial z \partial x} \\ &+ e_{323}\frac{\partial^2 u_y}{\partial z^2} - \varepsilon_{11}\frac{\partial^2 \varphi}{\partial x^2} - \varepsilon_{13}\frac{\partial^2 \varphi}{\partial x \partial z} - \varepsilon_{31}\frac{\partial^2 \varphi}{\partial z \partial x} - \varepsilon_{33}\frac{\partial^2 \varphi}{\partial z^2} = 0, \\ \frac{\partial T_{21}}{\partial x} &= C_{66}\frac{\partial^2 u_y}{\partial x^2} + C_{46}\frac{\partial^2 u_y}{\partial x \partial z} + e_{16}\frac{\partial^2 \varphi}{\partial x^2} + e_{36}\frac{\partial^2 \varphi}{\partial z \partial x}, \\ \frac{\partial T_{23}}{\partial z} &= C_{46}\frac{\partial^2 u_y}{\partial z \partial x} + C_{44}\frac{\partial^2 u_y}{\partial z^2} + e_{14}\frac{\partial^2 \varphi}{\partial z \partial x} + e_{34}\frac{\partial^2 \varphi}{\partial z^2}.\end{aligned} \tag{4}$$

Considering the system to be infinite in the x direction, we solved our equations over a finite computation domain of width a which is the period of the system [Fig. 1(a)]. Then, for a harmonic solution, the wave functions u_y and φ can be expressed as $u_y = U_y(x, z)e^{i(kx-\omega t)}$ and $\varphi = \Phi(x, z)e^{i(kx-\omega t)}$, where ω is the angular frequency, k is the complex wavenumber, and U_y and Φ verify the Bloch–Floquet condition $U_y(x + a, y) = U_y(x, y)$ and $\Phi(x + a, y) = \Phi(x, y)$.[19] The governing equations can then be solved over the domain defined by $0 \le x \le a$. Equation (4) becomes

$$\begin{aligned}-\rho U_y\omega^2 &= C_{66}\frac{\partial^2 U_y}{\partial x^2} + 2ikC_{66}\frac{\partial U_y}{\partial x} - k^2 C_{66}U_y + C_{64}\frac{\partial^2 U_y}{\partial x \partial z} \\ &+ ikC_{64}\frac{\partial U_y}{\partial z} + C_{46}\frac{\partial^2 U_y}{\partial z \partial x} + ikC_{64}\frac{\partial U_y}{\partial z} + C_{44}\frac{\partial^2 U_y}{\partial z^2} \\ &+ e_{16}\frac{\partial^2 \Phi}{\partial x^2} + 2ike_{16}\frac{\partial \Phi}{\partial x} - k^2 e_{16}\Phi + e_{36}\frac{\partial^2 \Phi}{\partial z \partial x} \\ &+ ike_{36}\frac{\partial \Phi}{\partial x} + e_{14}\frac{\partial^2 \Phi}{\partial z \partial x} + ike_{14}\frac{\partial \Phi}{\partial z} + e_{34}\frac{\partial^2 \Phi}{\partial z^2}\end{aligned} \tag{5}$$

and

$$\begin{aligned}&e_{16}\frac{\partial^2 U_y}{\partial x^2} + 2ike_{16}\frac{\partial U_y}{\partial x} - k^2 e_{16}U_y + e_{14}\frac{\partial^2 U_y}{\partial x \partial z} + ike_{14}\frac{\partial U_y}{\partial z} + e_{36}\frac{\partial^2 U_y}{\partial z \partial x} \\ &+ ike_{36}\frac{\partial U_y}{\partial z} + e_{34}\frac{\partial^2 U_y}{\partial z^2} - \varepsilon_{11}\frac{\partial^2 \Phi}{\partial x^2} - 2ik\varepsilon_{11}\frac{\partial \Phi}{\partial x} + k^2\,\varepsilon_{11}\Phi \\ &- \varepsilon_{13}\frac{\partial^2 \Phi}{\partial x \partial z} - ik\varepsilon_{13}\frac{\partial \Phi}{\partial z} - \varepsilon_{31}\frac{\partial^2 \Phi}{\partial z \partial x} - ik\varepsilon_{31}\frac{\partial \Phi}{\partial z} - \varepsilon_{33}\frac{\partial^2 \Phi}{\partial z^2} = 0.\end{aligned} \tag{6}$$

Meanwhile, the GL is considered isotropic and non-piezoelectric with shear modulus μ_{GL}. Thus, from Eq. (2), we can obtain the following governing equation in the GL:

$$-\rho U_y\omega^2 = \mu_{GL}\left(\frac{\partial^2 U_y}{\partial x^2} + \frac{\partial^2 U_y}{\partial z^2}\right) + 2ik\mu_{Gl}\frac{\partial U_y}{\partial x} - \mu_{GL}k^2 U_y. \tag{7}$$

The shear modulus μ_{GL} corresponds to the first Lamé coefficient can be obtained by $\mu_{GL} = C_{44} = (C_{11} - C_{12})/2$ for an isotropic material.

Regarding the viscous fluid layer, where the fluid is considered Newtonian, we use the same Eq. (7) as the GL with the dynamic viscosity term η_L in the shear modulus. According to the Voigt model, viscosity intervenes in the expression of the complex shear modulus,[20,21]

$$\mu_L^* = g' + ig'', \tag{8}$$

where $g' = 0$ and $g'' = \eta_L\omega$.

The set of equations (5)–(7) can be then formulated into a quadratic eigenvalue problem where the eigenvalue is the complex wavenumber k. To solve these equations, they were implemented as a polynomial equation in the PDE module of the commercial software Comsol Multiphysics® 5.3a,

$$0 = A\boldsymbol{U} + k^2 e_a\boldsymbol{U} - kd_a\boldsymbol{U} - C\nabla^2\boldsymbol{U} + \beta\nabla\boldsymbol{U}, \tag{9}$$

where the wavenumber k is the eigenvalue, and the vector $\boldsymbol{U}$ is constructed by introducing the derivatives of U_y and Φ,

$$\boldsymbol{U} = \left[\ U_y,\quad \frac{\partial U_y}{\partial x},\quad \frac{\partial U_y}{\partial z},\quad \Phi,\quad \frac{\partial \Phi}{\partial x},\quad \frac{\partial \Phi}{\partial z}\ \right]^T. \tag{10}$$

The matrices A, e_a, d_a, C, and β are expressed in the Appendix. The solving process was performed over the domain presented in Fig. 1(a) where the substrate has finite depth with its bottom boundary being constrained to zero displacement field. The domain width a is estimated to be half the wavelength, $a = \lambda_L/2 = V_L/2f$, where f is the operating frequency and V_L is the speed of Love waves for the case of a substrate and GL without the fluid. We took the estimation of $V_L = \sqrt{V_S V_{GL}}$ with V_S and V_{GL} the speed of shear waves in the substrate and the guiding layer, respectively. For instance, for the case of an SiO_2 guiding layer on a quartz substrate, $V_{GL} = 3009.3$ m/s and $V_S = \sqrt{(C_{66} + e_{34}^2/\varepsilon_{33})/\rho_s} = 5052.2$ m/s (where C_{66}, e_{34}, ε_{33}, and ρ_s are the coefficients of the substrate), which gives $V_L = 3899.2$ m/s. Then, for a frequency of 250 MHz as chosen in this study, $a = 7.8\,\mu$m. Besides, the length of the substrate and the fluid domains are taken to be $10a$ and $2a$, respectively, which are sufficient considering the confinement of Love waves.

For the boundary conditions between the piezoelectric substrate and the GL, we have the continuity of the displacement field, the stress components T_{i3}, the electrical potential φ, and the normal component of the electrical displacement D_z,[22]

$$\begin{aligned}u_y^S|_{z=-w} &= u_y^{GL}|_{z=-w} \text{ and } T_{i3}^S|_{z=-w} = T_{i3}^{GL}|_{z=-w}, \\ \varphi_y^S|_{z=-w} &= \varphi_y^{GL}|_{z=-w} \text{ and } D_z^S|_{z=-w} = D_z^{GL}|_{z=-w}.\end{aligned} \tag{11}$$

For the interface between the fluid and the guiding layer ($z = 0$), along with the continuity of u_y, φ, and D_z, we only considered the continuity of the normal stress T_{33}, while the shear stress is zero,

$$T_{i3}^{GL}|_{z=0} = 0 \text{ for i } = 1,\ 2. \tag{12}$$

Furthermore, as the Comsol eigenvalue solver provides multiple solutions, our solution of interest corresponding to a Love wave

TABLE I. Properties of quartz ST-cut, LiNbO3 Y128°-cut, SiO_2 and water.[21]

Parameter	Unit	Quartz ST-cut	$LiNbO_3$ Y128°-cut	SiO_2	Water
c_{44}	10^{10} N/m^2	3.033	7.805	1.995	
c_{64}		−0.761	0		
c_{66}		6.746	7.576		
e_{16}	C/m^2	0.099	−0.6162		
e_{36}		0.1071	0		
e_{14}		0	0		
e_{34}		0.0720	−2.2779		
e_{15}		0	0		
e_{35}		0	2.9156		
ε_{11}	10^{-11} F m	4.0171	30.7033	3.718	69.51
ε_{13}		−0.897	0	0	0
ε_{33}		4.0029	38.9	3.718	69.51
P	kg/m^3	2648	4700	2203	1000
H	Pa s				0.089

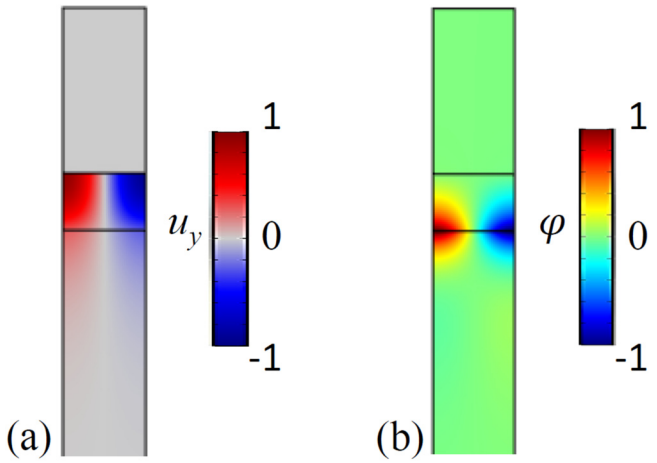

FIG. 2. Numerical evaluation of the displacement field u_y (a) and the electric field φ (b).

is selected by computing the following parameter:

$$SP = \frac{\int_{-w\le y\le 0}|U_y|^2}{\int_{y\le 0}|U_y|^2}. \tag{13}$$

The parameter SP compares the average of the displacement amplitude in the GL ($-w \le y \le 0$) with the total average displacement amplitude over the computation domain ($y \le 0$). For Love waves, knowing that the displacement field is mostly confined within the GL while it vanishes in the bulk substrate far from the surface, the quantity $\int_{-w\le y\le 0}^{0}|U_y|^2$ will be close to $\int_{y\le 0}|U_y|^2$, meaning that the value of SP will be close to 1. For the case of bulk modes, SP will be much smaller than 1 as the displacement field is distributed all over the entire domain.

The model was first used to study Love wave dispersion and attenuation in a three-layer system composed of a ST-cut quartz substrate, a silicon dioxide (SiO_2) GL, and a viscous fluid layer. The used materials' properties are listed in Table I.

As the geometry of the model is of rectangular shape, we used a square mesh distribution. Figure 2 shows the displacement and electrical fields confinement in the GL for the Love wave calculated by our numerical model. We evaluated the phase velocity and attenuation using the following equations:

$$V_L = \frac{\omega}{\mathrm{Re}(k)},$$
$$\text{Attenuation} = \mathrm{Im}(k). \tag{14}$$

III. RESULTS AND DISCUSSION

We first compared the results of our FE based model with the ones provided by the analytical model developed by Kiełczyński for a Love wave propagating in a three-layer structure.[14] Kiełczyński's model considered the substrate isotropic and did not take into account the piezoelectricity. We made different simulations varying the thickness of the guiding layer, the viscosity of the fluid, and the frequency of the wave.

Under water loading, we first studied the phase velocity and wave attenuation as a function of the GL thickness at an operating frequency of 250 MHz [Fig. 3(a)] and as a function of the frequency for a fixed GL thickness of 4.2 μm [Fig. 3(b)]. For both cases, we observe a good agreement between the analytical results from Kiełczyński's model (solid lines) and our numerical ones (circular dots). The phase velocity of Love waves decreases as we increase the thickness of the GL, while the attenuation experiences a maximum around 3.8 μm which corresponds to a third of the wavelength. At this thickness, the attenuation reaches a maximum of 800 Np/m in water. As our model takes into account the piezoelectricity (in contrast to Kiełczyński's model), we can confirm that piezoelectricity has a slight influence on the phase velocity (blue curves) for a thickness w below 2.2 μm at 250 MHz [Fig. 3(a)] and for $w = 4.2\,\mu$m below 150 MHz [Fig. 3(b)]. Also, piezoelectricity has a slight influence on the wave attenuation (red curves) for thickness w greater than 2.3 μm at 250 MHz and for $w = 4.2\,\mu$m above 90 MHz. Hence, Kiełczyński's model nevertheless gives a good approximation for the phase velocity and attenuation when neglecting piezoelectricity.

We also compared our numerical results with those provided by the simplified model of Kiełczyński[14] for the case of evaluating the wave velocity and attenuation as a function of the fluid viscosity for a GL thickness of 4.2 μm at 250 MHz (Fig. 4). For low viscosities, a good match is observed between the two models which confirms the results obtained for water (viscosity of 0.089 Pa s) [Fig. 3(b)]. However, the two models diverge for viscosity values higher than 1 Pa s and 2.5 Pa s for the phase velocity and attenuation, respectively, as can be seen in Fig. 4. Compared with our model, Kiełczyński's model tends to significantly overestimate the Love wave

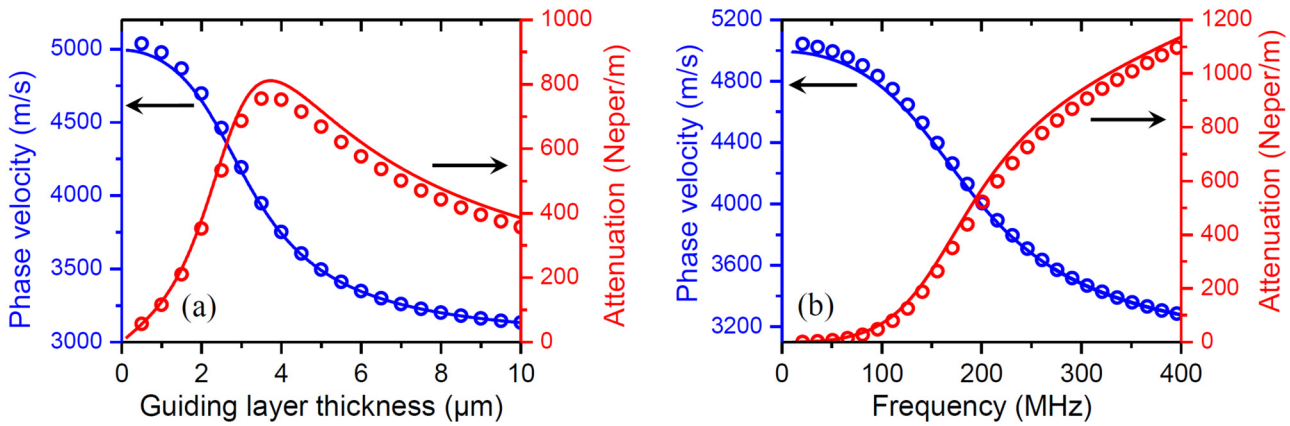

FIG. 3. Evolution of Love wave phase velocity (blue) and attenuation (red) under water loading as a function of (a) the GL thickness w at 250 MHz and (b) the frequency for $w = 4.2\,\mu$m. Kiełczyński's model (solid line) and numerical model (open dots).

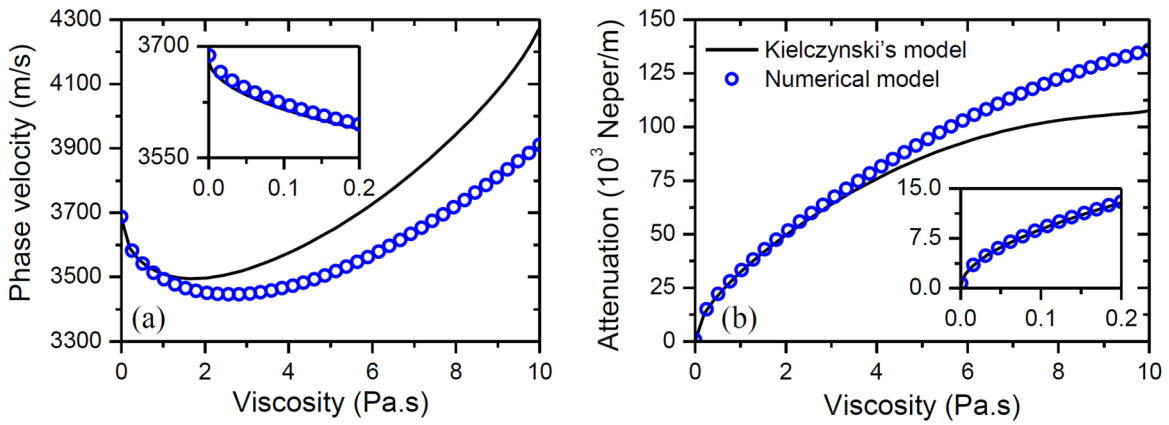

FIG. 4. Evolution of Love wave velocity (a) and attenuation (b) as a function of the fluid layer viscosity using Kiełczyński's model (solid line) and our numerical model (circular dots), with enlargement in the range of small viscosity (insets).

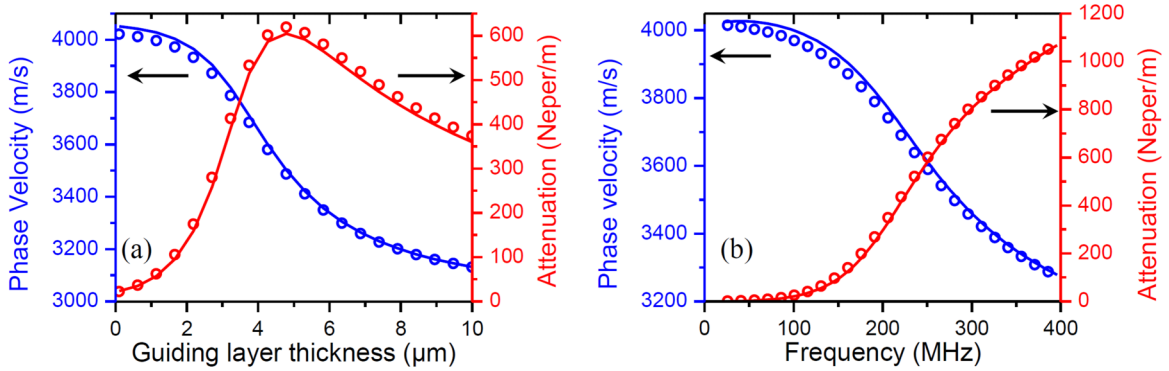

FIG. 5. Evolution of Love wave phase velocity (red) and attenuation (blue) in $LiNbO_3$ as a function of the thickness w of the guiding layer at 250 MHz (a) and frequency for $w = 4.2\,\mu$m (b) under water, with piezoelectricity (solid line) and without piezoelectricity (circular dots).

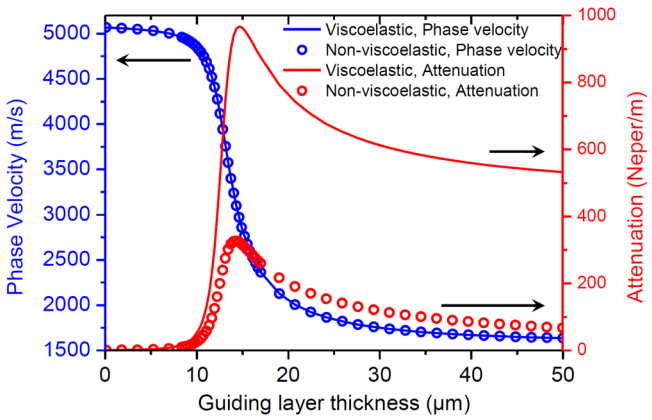

FIG. 6. Evolution of Love wave velocity and attenuation in the quartz substrate with SU-8 polymeric GL under water as a function of the thickness of the GL w with (solid line) and without (circular dots) viscoelasticity, at 250 MHz.

phase velocity (and thus underestimate the wave's attenuation) under highly viscous fluid. Our numerical model increases the accuracy of evaluating the wave velocity and attenuation for high values of viscosity while Kiełczyński's model is still applicable for low values of viscosity (below 1 Pa s).

In a second study, we used our model to investigate the Love wave dispersion and attenuation in a system made of $LiNbO_3$ Y128° substrate (Table I) with a SiO_2 guiding layer, under a viscous liquid (water). To the best of our knowledge, no study has been conducted to investigate the wave phase velocity and attenuation in such a well-known and commonly used material in SAW based devices.[23–25] Love wave velocity and attenuation are plotted in Fig. 5 as a function of the GL thickness at 250 MHz [Fig. 5(a)] and as a function of the operating frequency for $w = 4.2\,\mu$m, depending on considering (solid line) or neglecting (circular dots) the piezoelectricity of the substrate. Similarly to quartz, we observe that the piezoelectricity of $LiNbO_3$ has slightly some effect on the wave velocity when considering GL thickness lower than 3 μm at 250 MHz [Fig. 5(a)] and for frequencies lower than 250 Hz for a 4.2 μm thick GL [Fig. 5(b)]. The piezoelectric effect of the $LiNbO_3$ Y128 substrate has to be taken into account when evaluating the Love wave velocity in this kind of system. Besides, piezoelectricity has almost no effect on the wave attenuation.

Besides, we have also investigated the case of considering a viscoelastic GL such as SU-8, a material extensively used in micro/nanofabrication, and widely applied as a GL for Love waves[26–28] for the purpose of bio-sensing application. For this material, the viscoelasticity was introduced by considering the frequency dependent imaginary part of the shear modulus[29] [Eq. (15)]. It is then crucial to investigate the effect of the polymer viscoelasticity on the Love wave propagation,

$$\mu^*_{GL} = \mu_{GL} + i\eta_{GL}\omega. \tag{15}$$

For the SU-8, we consider $\mu_{GL} = 3$ GPa, $\eta_{GL} = 0.12$ Pa s, and $\rho_{GL} = 1200$ kg/m^3.[30,31] Figure 6 presents the effect of the viscoelasticity on the phase velocity and wave attenuation for

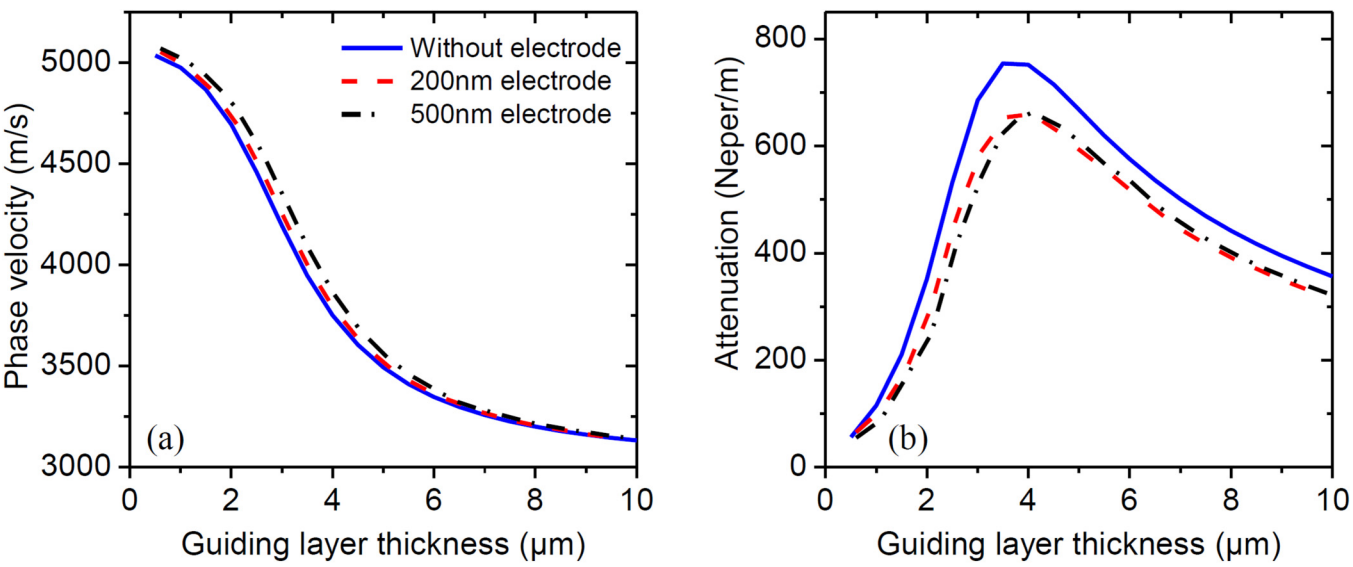

FIG. 7. Evolution of phase velocity (a) and attenuation (b) in the case of the quartz substrate with silica GL under water as a function of the thickness of the GL at 250 MHz, for the case without electrode (solid blue line), and the case of electrode of 200 nm (red doted and dashed line) and 500 nm thickness (black dashed line).

the L-SAW multilayered structure made of quartz substrate, SU-8 GL, and water. For the sake of comparison, we also plotted the results for the case where the viscoelasticity is neglected ($\eta_{GL} = 0$) (circular dots). The polymer viscoelasticity does not affect the wave velocity while it greatly increases the attenuation of the Love waves in the structure. This shows the importance of considering the viscoelastic properties of soft polymeric materials used as a GL for the optimization of Love waves based devices.

We took advantage of our numerical model to push further our study by investigating the Love wave dispersion and attenuation for the multilayered system that includes an electrode [Fig. 1(b)], which constitutes a close representation of the realistic system. To the best of our knowledge, no theoretical investigation has been conducted for this case which is relatively complicated to handle using classical analytical formulations. For the study, two electrode thicknesses commonly used in SAW devices (200 and 500 nm) were considered. At 250 MHz [Fig. 7(a)], we first observe that the presence of the electrode has a relatively negligible effect on the phase velocity for GL thickness above 6 μm, for which the electrode thickness of 500 nm represents 8.33% of the GL thickness. However, for GL thickness below 6 μm, the effect of the electrode on the phase velocity is distinguishable, though the maximum velocity shift is still below 2.5%. We can then conclude that the thickness of the electrodes has little effect on the phase velocity of the L-SAW. Besides, the situation seems to be different for the attenuation [Fig. 7(b)] where except for thin guiding layers (<1 μm), the presence of the electrode significantly affects the wave attenuation. The case without the electrode (solid blue curve) gives an over estimation (around 30%) of the Love wave attenuation compared to the case with the electrode (red and black lines). Thus, the electrode has to be included in the modeling process of L-SAW, as it effects significantly the wave attenuation.

IV. CONCLUSION

We have presented a FE based model to characterize the Love wave propagation in a multilayered system made of an anisotropic piezoelectric substrate and a viscoelastic GL under a viscous fluid. The model is based on calculating the complex wavenumber as an eigenvalue in the wave equation, from which the phase velocity and wave attenuation can be evaluated. The model offers great flexibility by considering the materials anisotropy, piezoelectricity, and viscoelasticity under viscous fluid at any frequency range. Furthermore, a strong feature of the model is its capability of handling complex geometries such as considering the electrode to investigate their influence on the wave velocity and attenuation. Regarding the Love wave dispersion, we have shown that the substrate piezoelectricity should not be neglected at some specific ranges of frequencies and GL thicknesses. Besides, the GL viscoelasticity does not affect the wave velocity while it attenuates greatly the wave. The present FE based model is not limited to the studied systems in this work but can also be used for other multilayered structures and materials without changing the formulation of the equations. The model would help improve the optimization of Love waves based devices and enable extending the studies on a wide range of anisotropic and piezoelectric materials with random topological surface.

ACKNOWLEDGMENTS

M.O. and F.S. would like to thank the CNES (Centre National d'Etudes Spatiales) and the CNRS (Centre National de la Recherche Scientifique) for financial support.

APPENDIX: MATRIX EXPRESSIONS FOR THE EIGENVALUE PROBLEM

By comparing Eqs. (5)–(9) in order to identify the parameters, we obtain

$$\begin{aligned} A\boldsymbol{U} &= \rho U_y \omega^2, \; -C\nabla^2\boldsymbol{U} = C_{66}\frac{\partial^2 U_y}{\partial x^2} + C_{44}\frac{\partial^2 U_y}{\partial z^2} + e_{16}\frac{\partial^2 \Phi}{\partial x^2} \\ &\quad + e_{34}\frac{\partial^2 \Phi}{\partial z^2} + C_{64}\frac{\partial^2 U_y}{\partial x \partial z} + C_{46}\frac{\partial^2 U_y}{\partial z \partial x} + e_{36}\frac{\partial^2 \Phi}{\partial z \partial x} + e_{14}\frac{\partial^2 \Phi}{\partial z \partial x}, \\ \lambda^2 e_a \boldsymbol{U} &= -k^2 C_{66} U_y - k^2 e_{16}\Phi, \; -\lambda d_a \boldsymbol{U} = 2ike_{16}\frac{\partial \Phi}{\partial x} + ike_{36}\frac{\partial \Phi}{\partial x} \\ &\quad + ike_{14}\frac{\partial \Phi}{\partial z} + 2ikC_{64}\frac{\partial U_y}{\partial z} + 2ikC_{66}\frac{\partial U_y}{\partial x}. \end{aligned} \tag{A1}$$

By rearranging Eq. (8) in order to identify the parameters, we obtain

$$\begin{aligned} -C\nabla^2\boldsymbol{U} &= e_{16}\frac{\partial^2 U_y}{\partial x^2} + e_{34}\frac{\partial^2 U_y}{\partial z^2} - \varepsilon_{11}\frac{\partial^2 \Phi}{\partial x^2} - \varepsilon_{33}\frac{\partial^2 \Phi}{\partial z^2} + e_{14}\frac{\partial^2 U_y}{\partial x \partial z} \\ &\quad + e_{36}\frac{\partial^2 U_y}{\partial z \partial x} - \varepsilon_{13}\frac{\partial^2 \Phi}{\partial x \partial z} - \varepsilon_{31}\frac{\partial^2 \Phi}{\partial z \partial x}, \\ \lambda^2 e_a \boldsymbol{U} &= -k^2 e_{16} U_y + k^2 \varepsilon_{11}\Phi, \; -\lambda d_a \boldsymbol{U} = -2ik\varepsilon_{11}\frac{\partial \Phi}{\partial x} \\ &\quad + ike_{14}\frac{\partial U_y}{\partial z} + ike_{36}\frac{\partial U_y}{\partial z} - ik\varepsilon_{13}\frac{\partial \Phi}{\partial z} - ik\varepsilon_{31}\frac{\partial \Phi}{\partial z} \\ &\quad + 2ike_{16}\frac{\partial U_y}{\partial x} \end{aligned} \tag{A2}$$

then the matrices implemented in Comsol Multiphysics for the piezoelectric layer are

$$C=\begin{bmatrix} \begin{bmatrix} -C_{66} & -C_{46} \\ -C_{46} & -C_{44} \end{bmatrix} & \begin{matrix} 0 & 0 \\ 0 & 0 \end{matrix} & \begin{bmatrix} -e_{16} & -e_{36} \\ -e_{14} & -e_{34} \end{bmatrix} & \begin{matrix} 0 & 0 \\ 0 & 0 \end{matrix} \\ \begin{matrix} 0 \\ 0 \end{matrix} & \begin{matrix} 0 & 0 \\ 0 & 0 \end{matrix} & \begin{matrix} 0 \\ 0 \end{matrix} & \begin{matrix} 0 & 0 \\ 0 & 0 \end{matrix} \\ \begin{bmatrix} -e_{16} & -e_{14} \\ -e_{36} & -e_{34} \end{bmatrix} & \begin{matrix} 0 & 0 \\ 0 & 0 \end{matrix} & \begin{bmatrix} \varepsilon_{11} & \varepsilon_{13} \\ \varepsilon_{13} & \varepsilon_{33} \end{bmatrix} & \begin{matrix} 0 & 0 \\ 0 & 0 \end{matrix} \\ \begin{matrix} 0 \\ 0 \end{matrix} & \begin{matrix} 0 & 0 \\ 0 & 0 \end{matrix} & \begin{matrix} 0 \\ 0 \end{matrix} & \begin{matrix} 0 & 0 \\ 0 & 0 \end{matrix} \end{bmatrix}, A=\begin{bmatrix} \rho\omega^2 & 0 & 0 & 0 & 0 & 0 \\ 0 & 1 & 0 & 0 & 0 & 0 \\ 0 & 0 & 1 & 0 & 0 & 0 \\ 0 & 0 & 0 & 1 & 0 & 0 \\ 0 & 0 & 0 & 0 & 1 & 0 \\ 0 & 0 & 0 & 0 & 0 & 1 \end{bmatrix}, e_a=\begin{bmatrix} -C_{66} & 0 & 0 & -e_{16} & 0 & 0 \\ 0 & 0 & 0 & 0 & 0 & 0 \\ 0 & 0 & 0 & 0 & 0 & 0 \\ -e_{16} & 0 & 0 & \varepsilon_{11} & 0 & 0 \\ 0 & 0 & 0 & 0 & 0 & 0 \\ 0 & 0 & 0 & 0 & 0 & 0 \end{bmatrix},$$

$$d_a=\begin{bmatrix} 0 & 2i & -2i & 0 & -3i & -i \\ 0 & 0 & 0 & 0 & 0 & 0 \\ 0 & 0 & 0 & 0 & 0 & 0 \\ 0 & 2i & -2i & 0 & 2i & 2i \\ 0 & 0 & 0 & 0 & 0 & 0 \\ 0 & 0 & 0 & 0 & 0 & 0 \end{bmatrix}, \beta=\begin{bmatrix} \begin{bmatrix} 0 \\ 0 \end{bmatrix} & \begin{bmatrix} -2C_{66} \\ 0 \end{bmatrix} & \begin{bmatrix} 0 \\ 2C_{64} \end{bmatrix} & \begin{bmatrix} 0 \\ 0 \end{bmatrix} & \begin{bmatrix} 2e_{16}+e_{36} \\ 0 \end{bmatrix} & \begin{bmatrix} 0 \\ e_{14} \end{bmatrix} \\ \begin{bmatrix} 0 \\ 0 \end{bmatrix} & \begin{bmatrix} 0 \\ 0 \end{bmatrix} & \begin{bmatrix} 0 \\ 0 \end{bmatrix} & \begin{bmatrix} 0 \\ 0 \end{bmatrix} & \begin{bmatrix} 0 \\ 0 \end{bmatrix} & \begin{bmatrix} 0 \\ 0 \end{bmatrix} \\ \begin{bmatrix} 0 \\ 0 \end{bmatrix} & \begin{bmatrix} 0 \\ 0 \end{bmatrix} & \begin{bmatrix} 0 \\ 0 \end{bmatrix} & \begin{bmatrix} 0 \\ 0 \end{bmatrix} & \begin{bmatrix} 0 \\ 0 \end{bmatrix} & \begin{bmatrix} 0 \\ 0 \end{bmatrix} \\ \begin{bmatrix} 0 \\ 0 \end{bmatrix} & \begin{bmatrix} -2e_{16} \\ 0 \end{bmatrix} & \begin{bmatrix} 0 \\ e_{14}+e_{36} \end{bmatrix} & \begin{bmatrix} 0 \\ 0 \end{bmatrix} & \begin{bmatrix} -2\varepsilon_{11} \\ 0 \end{bmatrix} & \begin{bmatrix} 0 \\ -2\varepsilon_{13} \end{bmatrix} \\ \begin{bmatrix} 0 \\ 0 \end{bmatrix} & \begin{bmatrix} 0 \\ 0 \end{bmatrix} & \begin{bmatrix} 0 \\ 0 \end{bmatrix} & \begin{bmatrix} 0 \\ 0 \end{bmatrix} & \begin{bmatrix} 0 \\ 0 \end{bmatrix} & \begin{bmatrix} 0 \\ 0 \end{bmatrix} \\ \begin{bmatrix} 0 \\ 0 \end{bmatrix} & \begin{bmatrix} 0 \\ 0 \end{bmatrix} & \begin{bmatrix} 0 \\ 0 \end{bmatrix} & \begin{bmatrix} 0 \\ 0 \end{bmatrix} & \begin{bmatrix} 0 \\ 0 \end{bmatrix} & \begin{bmatrix} 0 \\ 0 \end{bmatrix} \end{bmatrix}. \quad \text{(A3)}$$

The matrices implemented in Comsol for the guiding layer are

$$C=\begin{bmatrix} -\mu_{GL} & 0 & 0 & 0 & 0 & 0 \\ 0 & 0 & 0 & 0 & 0 & 0 \\ 0 & 0 & 0 & 0 & 0 & 0 \\ 0 & 0 & 0 & \varepsilon_{GL} & 0 & 0 \\ 0 & 0 & 0 & 0 & 0 & 0 \\ 0 & 0 & 0 & 0 & 0 & 0 \end{bmatrix}, A=\begin{bmatrix} \rho\omega^2 & 0 & 0 & 0 & 0 & 0 \\ 0 & 1 & 0 & 0 & 0 & 0 \\ 0 & 0 & 1 & 0 & 0 & 0 \\ 0 & 0 & 0 & 1 & 0 & 0 \\ 0 & 0 & 0 & 0 & 1 & 0 \\ 0 & 0 & 0 & 0 & 0 & 1 \end{bmatrix}, e_a=\begin{bmatrix} -\mu_{GL} & 0 & 0 & 0 & 0 & 0 \\ 0 & 0 & 0 & 0 & 0 & 0 \\ 0 & 0 & 0 & 0 & 0 & 0 \\ 0 & 0 & 0 & \varepsilon_{GL} & 0 & 0 \\ 0 & 0 & 0 & 0 & 0 & 0 \\ 0 & 0 & 0 & 0 & 0 & 0 \end{bmatrix}, d_a=\begin{bmatrix} 0 & 0 & 0 & 0 & 0 & 0 \\ 0 & -2i & 0 & 0 & 0 & 0 \\ 0 & 0 & 0 & 0 & 0 & 0 \\ 0 & 0 & 0 & 0 & 2i & 0 \\ 0 & 0 & 0 & 0 & 0 & 0 \\ 0 & 0 & 0 & 0 & 0 & 0 \end{bmatrix},$$

$$\beta=\begin{bmatrix} \begin{bmatrix} 0 \\ 0 \end{bmatrix} & \begin{bmatrix} 0 \\ 0 \end{bmatrix} & \begin{bmatrix} 0 \\ 0 \end{bmatrix} & \begin{bmatrix} 0 \\ 0 \end{bmatrix} & \begin{bmatrix} 0 \\ 0 \end{bmatrix} & \begin{bmatrix} 0 \\ 0 \end{bmatrix} \\ \begin{bmatrix} 0 \\ 0 \end{bmatrix} & \begin{bmatrix} \mu_{GL} \\ 0 \end{bmatrix} & \begin{bmatrix} 0 \\ 0 \end{bmatrix} & \begin{bmatrix} 0 \\ 0 \end{bmatrix} & \begin{bmatrix} 0 \\ 0 \end{bmatrix} & \begin{bmatrix} 0 \\ 0 \end{bmatrix} \\ \begin{bmatrix} 0 \\ 0 \end{bmatrix} & \begin{bmatrix} 0 \\ 0 \end{bmatrix} & \begin{bmatrix} 0 \\ 0 \end{bmatrix} & \begin{bmatrix} 0 \\ 0 \end{bmatrix} & \begin{bmatrix} 0 \\ 0 \end{bmatrix} & \begin{bmatrix} 0 \\ 0 \end{bmatrix} \\ \begin{bmatrix} 0 \\ 0 \end{bmatrix} & \begin{bmatrix} 0 \\ 0 \end{bmatrix} & \begin{bmatrix} 0 \\ 0 \end{bmatrix} & \begin{bmatrix} 0 \\ 0 \end{bmatrix} & \begin{bmatrix} -2\varepsilon_{GL} \\ 0 \end{bmatrix} & \begin{bmatrix} 0 \\ 0 \end{bmatrix} \\ \begin{bmatrix} 0 \\ 0 \end{bmatrix} & \begin{bmatrix} 0 \\ 0 \end{bmatrix} & \begin{bmatrix} 0 \\ 0 \end{bmatrix} & \begin{bmatrix} 0 \\ 0 \end{bmatrix} & \begin{bmatrix} 0 \\ 0 \end{bmatrix} & \begin{bmatrix} 0 \\ 0 \end{bmatrix} \\ \begin{bmatrix} 0 \\ 0 \end{bmatrix} & \begin{bmatrix} 0 \\ 0 \end{bmatrix} & \begin{bmatrix} 0 \\ 0 \end{bmatrix} & \begin{bmatrix} 0 \\ 0 \end{bmatrix} & \begin{bmatrix} 0 \\ 0 \end{bmatrix} & \begin{bmatrix} 0 \\ 0 \end{bmatrix} \end{bmatrix}. \quad \text{(A4)}$$

The Matrices implemented in Comsol for the fluid layer are

$$C = \begin{bmatrix} -\mu_L & 0 & 0 & 0 & 0 & 0 \\ 0 & 0 & 0 & 0 & 0 & 0 \\ 0 & 0 & 0 & 0 & 0 & 0 \\ 0 & 0 & 0 & \varepsilon_f & 0 & 0 \\ 0 & 0 & 0 & 0 & 0 & 0 \\ 0 & 0 & 0 & 0 & 0 & 0 \end{bmatrix}, A = \begin{bmatrix} \rho\omega^2 & 0 & 0 & 0 & 0 & 0 \\ 0 & 1 & 0 & 0 & 0 & 0 \\ 0 & 0 & 1 & 0 & 0 & 0 \\ 0 & 0 & 0 & 1 & 0 & 0 \\ 0 & 0 & 0 & 0 & 1 & 0 \\ 0 & 0 & 0 & 0 & 0 & 1 \end{bmatrix},$$

$$e_a = \begin{bmatrix} -\mu_L & 0 & 0 & 0 & 0 & 0 \\ 0 & 0 & 0 & 0 & 0 & 0 \\ 0 & 0 & 0 & 0 & 0 & 0 \\ 0 & 0 & 0 & \varepsilon_f & 0 & 0 \\ 0 & 0 & 0 & 0 & 0 & 0 \\ 0 & 0 & 0 & 0 & 0 & 0 \end{bmatrix}, d_a = \begin{bmatrix} 0 & 0 & 0 & 0 & 0 & 0 \\ 0 & -2i & 0 & 0 & 0 & 0 \\ 0 & 0 & 0 & 0 & 0 & 0 \\ 0 & 0 & 0 & 0 & 2i & 0 \\ 0 & 0 & 0 & 0 & 0 & 0 \\ 0 & 0 & 0 & 0 & 0 & 0 \end{bmatrix},$$

$$\beta = \begin{bmatrix} \begin{bmatrix} 0 \\ 0 \end{bmatrix} & \begin{bmatrix} 0 \\ 0 \end{bmatrix} & \begin{bmatrix} 0 \\ 0 \end{bmatrix} & \begin{bmatrix} 0 \\ 0 \end{bmatrix} & \begin{bmatrix} 0 \\ 0 \end{bmatrix} & \begin{bmatrix} 0 \\ 0 \end{bmatrix} \\ \begin{bmatrix} 0 \\ 0 \end{bmatrix} & \begin{bmatrix} \mu_{GL} \\ 0 \end{bmatrix} & \begin{bmatrix} 0 \\ 0 \end{bmatrix} & \begin{bmatrix} 0 \\ 0 \end{bmatrix} & \begin{bmatrix} 0 \\ 0 \end{bmatrix} & \begin{bmatrix} 0 \\ 0 \end{bmatrix} \\ \begin{bmatrix} 0 \\ 0 \end{bmatrix} & \begin{bmatrix} 0 \\ 0 \end{bmatrix} & \begin{bmatrix} 0 \\ 0 \end{bmatrix} & \begin{bmatrix} 0 \\ 0 \end{bmatrix} & \begin{bmatrix} 0 \\ 0 \end{bmatrix} & \begin{bmatrix} 0 \\ 0 \end{bmatrix} \\ \begin{bmatrix} 0 \\ 0 \end{bmatrix} & \begin{bmatrix} 0 \\ 0 \end{bmatrix} & \begin{bmatrix} 0 \\ 0 \end{bmatrix} & \begin{bmatrix} 0 \\ 0 \end{bmatrix} & \begin{bmatrix} -2\varepsilon_f \\ 0 \end{bmatrix} & \begin{bmatrix} 0 \\ 0 \end{bmatrix} \\ \begin{bmatrix} 0 \\ 0 \end{bmatrix} & \begin{bmatrix} 0 \\ 0 \end{bmatrix} & \begin{bmatrix} 0 \\ 0 \end{bmatrix} & \begin{bmatrix} 0 \\ 0 \end{bmatrix} & \begin{bmatrix} 0 \\ 0 \end{bmatrix} & \begin{bmatrix} 0 \\ 0 \end{bmatrix} \\ \begin{bmatrix} 0 \\ 0 \end{bmatrix} & \begin{bmatrix} 0 \\ 0 \end{bmatrix} & \begin{bmatrix} 0 \\ 0 \end{bmatrix} & \begin{bmatrix} 0 \\ 0 \end{bmatrix} & \begin{bmatrix} 0 \\ 0 \end{bmatrix} & \begin{bmatrix} 0 \\ 0 \end{bmatrix} \end{bmatrix}. \quad \text{(A5)}$$

DATA AVAILABILITY

The data that support the findings of this study are available from the corresponding authors upon reasonable request.

REFERENCES

[1]A. Pohl, IEEE Trans. Ultrason. Ferroelectr. Freq. Control **47**, 317 (2000).
[2]A. Abdollahi, J. Zhongwei, and S. A. Arabshahi, IEEE Trans. Ultrason. Ferroelectr. Freq. Control **54**, 2446–2455 (2007).
[3]S. K. M. Richardson, V. R. Bhethanabotla, and S. K. R. S. Sankaranarayanan, in *Proceedings of IEEE Sensors* (Institute of Electrical and Electronics Engineers Inc., 2014), pp. 213–216.
[4]J. Du, G. L. Harding, J. A. Ogilvy, P. R. Dencher, and M. Lake, Sens. Actuators A **56**, 211 (1996).
[5]H. Wu, G. Zhao, H. Zu, J. H. C. Wang, and Q. M. Wang, in *IEEE International Ultrasonic Symposium (IUS)* (IEEE Computer Society, 2017).
[6]V. Blondeau-Patissier, W. Boireau, B. Cavallier, G. Lengaigne, W. Daniau, G. Martin, and S. Ballandras, Sensors **7**, 1992 (2007).
[7]L. Rana, R. Gupta, M. Tomar, and V. Gupta, Sens. Actuators, B **261**, 169 (2018).
[8]J. Du and G. L. Harding, Sens. Actuators, A **65**, 152 (1998).
[9]G. McHale, F. Martin, and M. I. Newton, J. Appl. Phys. **92**, 3368 (2002).
[10]H. Oh, W. Wang, K. Lee, and S. Yang, in *Microfluidics, BioMEMS, and Medical Microsystems VII*, edited by W. Wang (SPIE, 2009), p. 72070R.
[11]T. Wang, R. Murphy, J. Wang, S. S. Mohapatra, S. Mohapatra, and R. Guldiken, Sensors **19**, 4533 (2019).
[12]P. Kiełczyński, M. Szalewski, and A. Balcerzak, Int. J. Solids Struct. **49**, 2314 (2012).
[13]A. Vikström and M. V. Voinova, Sens. Bio-Sens. Res. **11**, 78 (2016).
[14]P. Kiełczyński, Appl. Math. Model. **53**, 419 (2018).
[15]G. McHale, M. I. Newton, and F. Martin, J. Appl. Phys. **91**, 5735 (2002).
[16]J. Liu, AIP Adv. **4**, 077102 (2014).
[17]M. Oudich and M. Badreddine Assouar, J. Appl. Phys. **112**, 104509 (2012).
[18]D. Royer and E. Dieulesaint, *Elastic Waves in Solids I—Free and Guided Propagation|DANIEL ROYER* (Springer, 2000).
[19]P. Gómez García and J. P. Fernández-Álvarez, Math. Probl. Eng. **2015**, 475364 (2015).
[20]G. Madja, R. C. Y. Chin, and F. E. Followill, Geophys. J. Int. **80**, 1 (1985).
[21]R. M. Christensen, *Theory of Viscoelasticity* (Elsevier, 1982).
[22]J. Liu and S. He, Int. J. Solids Struct. **47**, 169 (2010).
[23]D. Cullen, G. Meltz, and T. Grudkowski, Appl. Phys. Lett. **44**, 182 (1984).
[24]F. S. Hickemell, H. D. Knuth, R. C. Dablemont, and T. S. Hickernell, in *IEEE International Ultrasonic Symposium* (IEEE, 1995), pp. 345–348.
[25]J. H. Sun and J. H. Jhou, Jpn. J. Appl. Phys. **53**, 07KB04 (2014).
[26]J. D. Ferry, *Viscoelastic Properties of Polymers*, 3rd ed. (Wiley, 1980).
[27]A. Del Campo and C. Greiner, J. Micromech. Microeng. **17**, R81 (2007).
[28]L. Jiang, J. Hossenlopp, R. Cernosek, and F. Josse, in *Proceedings of the Annual IEEE International Frequency Control Symposium* (IEEE, 2003), pp. 986–992.
[29]P. Roach, S. Atherton, N. Doy, G. McHale, and M. Newton, Sensors **7**, 2539 (2007).
[30]Z. Jie, J. Cheng, C. Ye, L. Honglang, and H. Shitang, in *Proceedings of the IEEE Ultrasonics Symposium* (IEEE, 2008), pp. 1120–1123.
[31]L. El Fissi, J. M. Friedt, F. Chérioux, and S. Ballandras, Sens. Actuators B **144**, 23 (2010).